Available online at www.sciencedirect.com
ScienceDirect
Trans. Nonferrous Met. Soc. China 34(2024) 1470−1486
Transactions of Nonferrous Metals Society of China
www.tnmsc.cn

Surface modification of biodegradable Mg/HA composite by electrospinning of PCL/HA fibers coating: Mechanical properties, corrosion, and biocompatibility

M. SHAMSI, M. SEDIGHI, A. BAGHERI

School of Mechanical Engineering, Iran University of Science and Technology, Tehran, Iran

Received 20 November 2022; accepted 11 April 2023

Abstract: Mg/HA composite was fabricated using the stir-casting and extrusion processes and coated by electrospun PCL/HA fibers (2.5 and 5 wt.% HA) to enhance the corrosion resistance. The mechanical tests demonstrated an increment of 107% for the compressive yield strength of the composite (151 vs 73 MPa for pure magnesium). SEM, EDS, and XRD analysis illustrated that HA particles distribute in porous coatings. According to the polarization tests, all coated specimens show higher corrosion resistance compared to the uncoated ones. PCL coating reduces the corrosion current density of the sample by two orders of magnitude. The effectiveness of incorporating HA in the coatings was proved by polarization and in vitro corrosion tests. Employment of coatings and subsequent Ca−P layer formation prevents the penetration of simulated body fluid (SBF) and contact with the substrate, thus protecting the surface. PCL/2.5%HA coated sample has the lowest corrosion rate with an average value of 0.98 mm/a by a reduction of 81% compared to the uncoated composite in 14 d. Cell viability enhancement from 43% to 121% was achieved using PCL/2.5%HA coating according to 3 d 3-(4,5-dimethylthiazol-2-yl)-2,5-diphenyl tetrazolium bromide (MTT) results. In conclusion, Mg/HA composites coated with PCL/2.5%HA fibers appear promising for bioabsorbable implant applications.
Key words: magnesium composite; composite coating; biodegradability; hydroxyapatite; polycaprolactone (PCL) fibers

1 Introduction

Orthopedic implants are used to keep the fracture points fixed and help the joints move. These implants must have acceptable mechanical properties and biocompatibility. Cobalt−chromium-based alloys, stainless steel, and titanium are used as conventional implants. Besides their high mechanical strength and biocompatibility, they have good corrosion resistance. In other words, their structural strength remains stable in the body for a long time. However, these implants have the disadvantage of being permanent, necessitating subsequent surgery to remove them. Long-term use of these implants may lead to clinical complications, permanent discomfort, and dysfunction. Also, the mismatch between the elastic modulus of these metals and that of the bone causes stress shielding effect [1,2]. In recent years, biomedical research has mostly considered biodegradable implants with a degradation rate commensurate with bone healing. A biodegradable implant must be mechanically strong, non-biotoxic, and maintain its mechanical integrity to be suitable for load-bearing applications. Due to its superb biocompatibility, biodegradability, and near-bone elastic modulus, magnesium has become a preferred metal for temporary orthopedic implants. Magnesium-based materials also exhibit osteoconductive properties, reducing implant healing time [3,4].

Medical applications of magnesium and its

Corresponding author: M. SEDIGHI, Tel: +98-21-7491228, Fax: +98-21-77240488, E-mail: sedighi@iust.ac.ir
DOI: 10.1016/S1003-6326(24)66484-8

alloys are restricted by the relatively rapid corrosion of the materials in the physiological environment. The mechanical integrity of magnesium implants is lost before tissue regeneration, and hydrogen gas is generated, which poses risks to the patient and slows bone healing. Alkaline poisoning can also result from the rapid destruction of implants [5,6]. There are various proposed methods, such as alloying [7−9], mechanical work [10,11], and surface modification [12,13], to minimize the corrosion rate of magnesium implants. Research has revealed that HA in the metal matrix, due to proper bioactivity and bone-like structure, as well as reducing degradation, causes bone growth [14,15]. Mg/HA composites possess enhanced mechanical strength and biological activity [16−18].

Additionally, surface modification is one of the most effective methods for controlling corrosion and improving implant biocompatibility. Developing surface engineering techniques led to a wide range of surface coating methods [19−22]. As well as being used in various applications, such as drug delivery, polymers can be used as anti-corrosion coatings [23]. Also, HA and other bioceramics or hybrid coatings have widely shown a beneficial role in controlling magnesium corrosion [24−26]. The HA coatings combine corrosion resistance and antibacterial properties with other helpful materials such as silver [27]. An electrospun coating contains fibers with high porosity, surface-to-volume ratio, and similarity to the extracellular matrix [28−30]. Silver nanoparticles and drugs can be incorporated into electrospun fibers to improve biocompatibility and antibacterial properties as well as control degradation [31,32]. The porous coating can also pass gas bubbles caused by unavoidable corrosion, making it more stable [33]. The polymeric materials used to coat magnesium implants must be biodegradable and biocompatible. Natural polymers have elevated bioactivity, but synthetic polymers exhibit more excellent corrosion resistance. Polycaprolactone (PCL) is a biodegradable synthetic polymer with good physical, chemical, and biocompatibility properties [34−37].

HANAS et al [38] indicated that PCL nanofiber coating effectively controls degradation and improves the biocompatibility and biological activity of AZ31. KIM et al [39] proved that PCL/ZnO nanofiber coating lowers the corrosion rate and augments the biocompatibility of AZ31. HANAS et al [40] prepared the PCL/HA coated AZ31/HA metal matrix composite using the FSP method and electrospinning. The experiments demonstrated that the coating, together with controlling the degradation rate, helped create a thicker CaP layer and promoted adhesion and cell proliferation. REZK et al [41] concluded that coated AZ31 alloy with PCL/nHA−simvastatin nanofibers exhibits good corrosion resistance and bone tissue regeneration. BAKHSHESHI-RAD et al [42] presented that coating of Ta_2O_5 layer and PCL/MgO−Ag nanofibers by magnetron sputtering and electrospinning on Mg−Ca−Zn improves the corrosion resistance and the apatite formation. PANAHI et al [43] examined the effect of BG-containing PCL fiber coating of AZ91 alloy, and resulted in the degradation rate reduced from 3.15 mm/a (for bare metal) to 2.98 mm/a. NANDHINI et al [44] used PCL and curcumin-loaded PCL nanofibers coating for AZ91 alloy. A polarization test showed that 8 wt.% PCL nanofibers coated sample has the highest corrosion resistance. KARTHEGA et al [45] achieved satisfactory corrosion resistance and cell proliferation results using PCL/TiO_2 fibers on AM50 alloy.

In this study, PCL and PCL/HA fibers were coated on stir-cast Mg/HA composite by the electrospinning method. Firstly, the mechanical properties of the prepared composite were evaluated. Then, the bio-corrosion behavior of coated composite samples (PCL, PCL/2.5%HA, and PCL/5%HA) was investigated in the SBF. Polarization and in vitro corrosion test results for the coated samples were extracted and compared to uncoated pure magnesium, magnesium composite, and acid-treated composite samples. Also, cell studies were performed on the coated sample with the lowest corrosion rate and bare composite.

2 Experimental

2.1 Materials

Commercially pure magnesium (99.9 wt.% Mg, <0.002 wt.% Ag, 0.02 wt.% Mn, >0.002 wt.% Ca, 0.028 wt.% Al, 0.011 wt.% Fe, <0.015 wt.% Zn, >0.003 wt.% Cu, 0.002 wt.% Cd, and 0.021 wt.% Si) was used as matrix. HA particles synthesized from bovine bone with an average size of about 412 nm

were utilized as composite reinforcements. In this study, PCL pellets (80 kDa) were purchased from Sigma Aldrich, UK. Acetic acid, formic acid, and other chemical solutions were prepared with pure laboratory grade.

2.2 Fabrication of Mg/HA composite

The magnesium-based composite was fabricated by stir casting. In this process, pure magnesium (99.9 wt.%) and HA (2.5 wt.%) powder were used as the matrix and reinforcing phase, respectively. It was decided to use this content of reinforcement based on previous research [46] due to better performance in fatigue testing. Prior to casting, the surface of magnesium was cleaned with ethanol to degrease and remove impurities. The molten magnesium and hydroxyapatite particles were mixed mechanically using an impeller. They were then blended by a magnetic method while cooling to the solidification point. Argon gas was used to protect the magnesium composite from oxidation during the casting process. Cast samples were subjected to two steps of hot extrusion (5∶1 and 4∶1) at 350 °C to improve the mechanical properties and lower defects. Finally, circular specimens with a diameter of 10 mm and a thickness of 2 mm were prepared using the cutting and turning processes. SEM and EDS were used to investigate the distribution of HA reinforcing particles in the magnesium matrix.

2.3 Tensile and compressive tests

After fabricating composite and performing two extrusion steps, the tension and compression test specimens were machined according to ASTM E8 and E9 standards, respectively. Three samples for each test were employed and tested under quasi-static conditions using Santam−STM50 at room temperature. Then, the yield and ultimate strength, and failure strain results were reported as average.

2.4 Pre-treatment of Mg/HA composite surface

Samples were polished using SiC emery paper to 2000 grade and cleaned via acetone and ethanol to remove impurities. Next, the samples were immersed in 1 mol/L nitric acid for 40 s. The samples were then washed in distilled water and ethanol and dried at room temperature for 24 h. Then, the surface was studied through SEM and EDS. Further, the grain size distribution on the acid-etched surface was investigated by Image J software. Contact angle measurements were also performed at five locations with distilled water as the contact fluid.

2.5 Electrospinning

PCL (12 wt.%) was dissolved in acetic and formic acids (3:1, volume ratio). Also, the HA particles (2.5 and 5 wt.%) required for PCL/HA composite fibers were dispersed in the solution using an ultrasonic shaker. For the purposes of assessing the effect of the HA content on corrosion resistance, two different contents were used, 2.5% and 5%. Due to agglomeration and inappropriate electrospinning, amounts exceeding 5% were not employed. The solution was then stirred via a magnetic stirrer for 6 h to dissolve the PCL and form a stable suspension. The optimal parameters to form uniform fibers were found by altering process parameters. The voltage, feed rate, and tip to the collector plate distance were preferred to be 10 kV, 0.01 mL/min, and 10 cm, respectively. In this study, a G23 gauge needle was employed, and the process was performed with a laboratory electrospinning setup. An adhesion test was performed according to ASTM D3359 on electrospun samples for different process durations, and 1 h-coating with 4B grade was selected as a suitable coating. The fabrication and coating steps of the samples are shown schematically in Fig. 1.

2.6 Electrochemical corrosion test

The polarization corrosion experiments were performed by PAR−VersaSTAT using a cell containing SBF (prepared according to KOKUBO and TAKADAMA [47]) with a pH of 7.4 at (37±1) °C. The cell consisted of a working electrode (coated and bare samples), Hg/HgCl reference electrode, and a platinum counter electrode. To plot the Tafel curves, the voltage scanned from −2.5 to 0 V at a scan rate of 1 mV/s. The samples were pre-immersed in the SBF for 0.5 h before the test to stabilize the open-circuit voltage. For each test, 250 mL of the SBF was consumed. The corrosion potential, current density, and anodic and cathodic slopes were calculated for samples. Furthermore, the polarization resistance (R_p) for each sample was calculated according to Eq. (1) [48]:

$$R_p = \frac{\beta_a \cdot \beta_c}{2.303(\beta_a + \beta_c) J_{corr}} \quad (1)$$

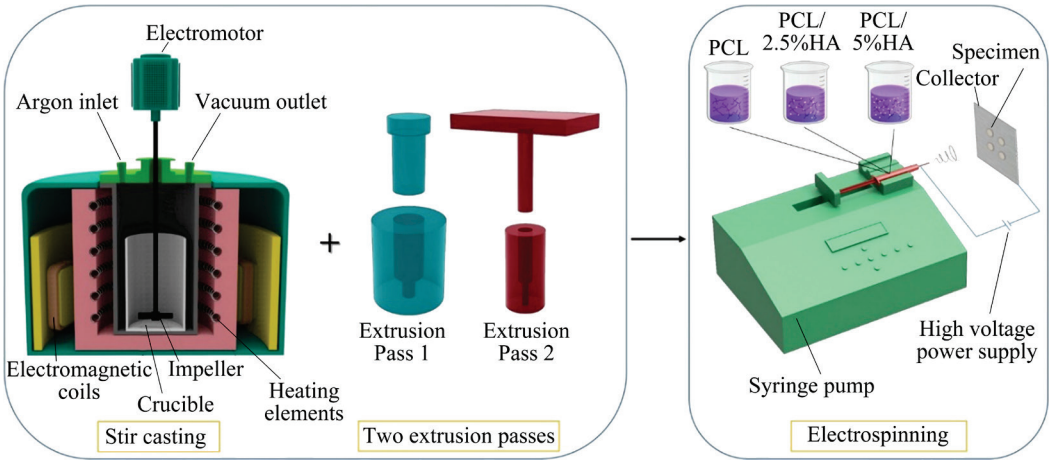

Fig. 1 Schematic picture of fabrication and coating steps of samples

where β_a and β_c are the slopes of the anodic and cathodic branches, respectively, in V/dec, and J_{corr} is the corrosion current density in μA/cm^2.

2.7 In-vitro degradation

The initial mass of the samples was recorded before the immersion. Next, the samples were immersed in SBF solution at (37±1) °C for 6, 12, 24, 72, 168, and 336 h. The pH values of media for each sample were assessed during immersion time. Moreover, an inverted graduated cylinder was placed on top of the samples (according to GAUR et al [49]) to measure the amount of hydrogen released during the degradation process. After immersion, the samples were air-dried, and their surface was analyzed by SEM and EDS. Then, they were washed with chromic acid and silver nitrate solution (200 g/L CrO_3 + 10 g/L $AgNO_3$) to remove corrosion products and other residuums. Finally, the samples were weighed, and the corrosion rate was calculated according to the mass difference [50]:

$$R_c = \frac{KW}{AtD} \quad (2)$$

where R_c is the corrosion rate in mm/a, K is the time conversion coefficient (8.76×10^4), W is the mass loss in g, A is the initial area of the sample in cm^2, t is the immersion time in h, and D is the density of magnesium (1.74 g/cm^3).

2.8 Cytotoxicity and cell culture study

An 3-(4,5-dimethylthiazol-2-yl)-2,5-diphenyl tetrazolium bromide (MTT) assay was used to test the viability of MC3T3-E1 cells (Pasteur Institute of Iran) on the PCL/2.5%HA coated and bare composites for 1 and 3 d. Several studies have employed these cells in the MTT assay [51−53]. The cells were cultured in a DMEM medium (Bio Idea, Iran) with 10% FBS (GIBCO, USA) and incubated in a medium with 95% humidity and 5% CO_2. Three of each sample were first sterilized with ethanol for 10 min, followed by UV for 40 min, and placed on a 24-well plate. Then, cells with a density of 5×10^4 per well were implanted, and the samples were incubated in 5% CO_2 at 37 °C for 1 and 3 d. 200 μL MTT solution was added at concentration of 0.5 mg/mL after the specified time intervals, and the cells were incubated for 4 h. By adding DMSO (Bio Idea, Iran) after removing MTT, the formed formazan crystals were solved, and the color intensity was measured by an ELISA reader (BioTek, USA) at 570 nm. Cell viability was calculated according to the optical density ratio of the test wells to the control.

In order to evaluate the adhesion and growth of MC3T3-E1 cells on the samples, these cells with a density of 1×10^5 per well were cultured on the sterilized samples inside a 12-well plate. After 1 and 3 d of incubation, they were fixed by PBS (GIBCO, USA) and 5 mL of 4 vol.% paraformaldehyde (DRM-CHEM, Iran) and then dehydrated with alcohol in concentrations of 50%−100%. After drying, the surface of the samples was gold coated and examined by an SEM microscope.

3 Results and discussion

3.1 Surface characterization

The proper distribution of hydroxyapatite particles in the magnesium matrix affects the

metallurgical, mechanical, and corrosion properties of the material. The yield and ultimate strength are affected by excessive local accumulation of powder and the formation of agglomerates due to defects and cavities. Also, the compressive failure strain illustrates significant reduction due to the micro-voids between the matrix and particles [54,55]. Proper distribution of HA in the matrix causes more uniform corrosion and weakens the occurrence of pitting. The cavities around the agglomerated area intensify biofluid penetration and, consequently, the corrosion rate [56,57]. Figure 2 presents the SEM image of the composite surface and the map of the elements. The white color on the surface indicates HA particles. A relatively good distribution of particles can be seen. Although in some areas, the presence of HA is in the form of webs, agglomeration in the casting process of metal composites is inevitable due to the low wettability of particles with small dimensions and large specific surface areas. However, this agglomeration is reduced by performing two extrusion steps on the parts [58]. The elemental analysis map in the white area proves the presence of the element Ca and P.

Figure 3 illustrates the SEM image and EDS result of etched surface of the magnesium composite and the grain size distribution diagram. The purpose of acid treatment was to create a porous $Mg(OH)_2$ to improve the adhesion of the coating. However, this layer protects the metal surface against corrosion [40,43]. The magnesium composite grains are revealed due to contact with the acid. Black dots and fibers can be seen, which are the vacancies of HA caused by HNO_3. The EDS diagram exhibits Ca, and P peaks with less intensity than the EDS diagram of intact composite (Fig. 2). The average ratio of Ca to P is about 1.67, which is close to that of HA. This indicates the presence of HA in the material structure after acidification. The grain size distribution of the magnesium composite

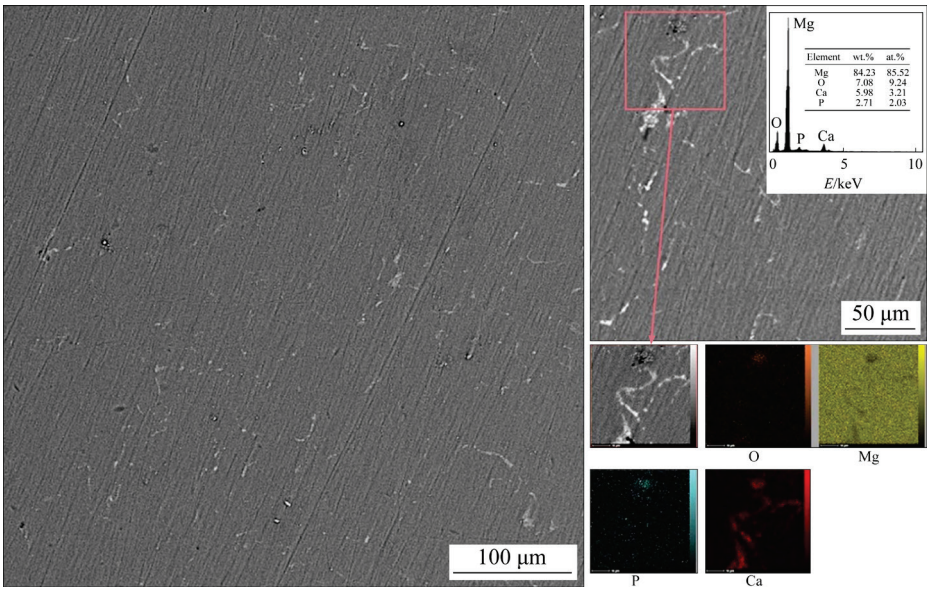

Fig. 2 SEM image of composite surface and scanning map of elements

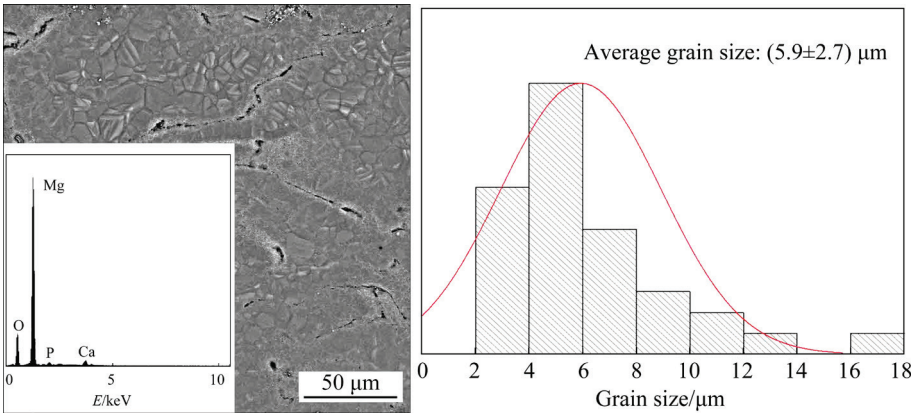

Fig. 3 SEM image and EDS result of etched surface of magnesium composite and grain size distribution diagram

surface is relatively uniform, and the average grain size is (5.9±2.7) μm.

Figure 4 shows the SEM images and EDS results of the coated surface of magnesium composite with PCL, PCL/2.5%HA, and PCL/5%HA, and fiber diameter distribution diagrams. The fibers are oriented relatively linearly and randomly and a porous structure is formed. PCL is widely used as a scaffold in tissue engineering due to its biodegradability and FDA approval. However, the formation of HA deposits on the PCL scaffold is complex due to its nature. Hence, electrospinning of this material combined with non-organic materials such as HA can create better bone repair properties [59,60]. White HA particles inside the PCL fibers can be seen in Figs. 4(b, c). Silver coating is used to improve SEM images, as indicated by the Ag peak in the EDS patterns. The EDS diagram shows the Ca and P peaks in these areas. The more delicate fibers create smaller pores for fluid to infiltrate and thus affect corrosion results. The average diameter of PCL fibers is (331±94.4) nm, which is diminished to be (309±102.77) nm with the addition of 2.5% HA in the PCL solution. This decrease could be related to the raised conductivity of the polymer solution due to HA particle inclusion. This increase in conductivity can boost electrical force, generating

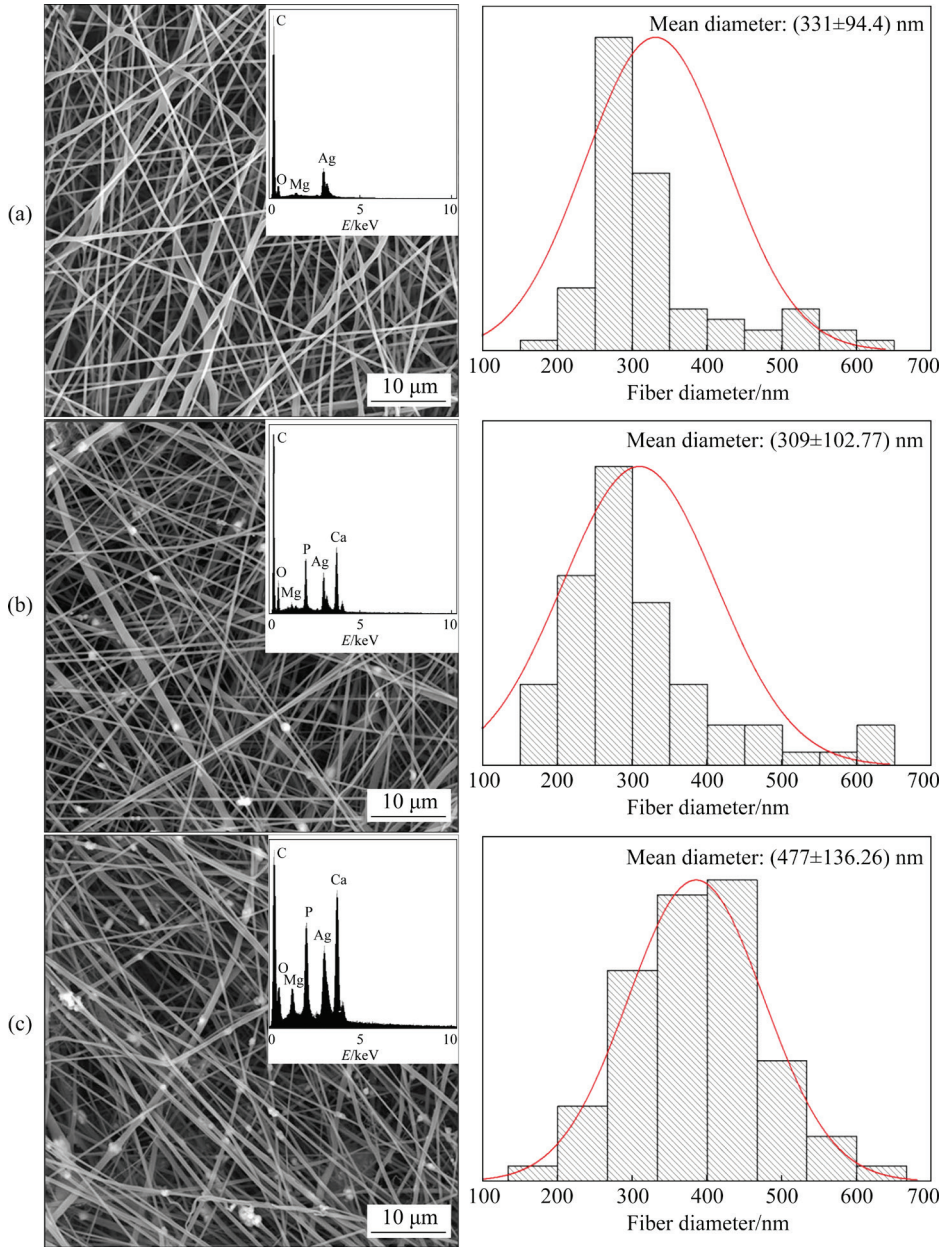

Fig. 4 SEM images, EDS results of coated surface and fiber diameter distribution diagrams of magnesium composite with PCL (a), PCL/2.5%HA (b), and PCL/5%HA (c)

thinner fibers [61]. As the mass fraction of HA rises from 2.5% to 5%, agglomeration of these particles within the fibers can be seen in several zones. As a result, bead formation and fiber diameter enlargement can be expected. Therefore, the average diameter of PCL/5%HA fibers is augmented to (477±136.26) nm.

The XRD patterns for samples are depicted in Fig. 5. Magnesium peaks with different intensities can be seen in all samples. The HA peaks are not clearly visible in composite and acid-treated composite due to their lower value. However, a peak at 2θ of about 43° is seen in all samples except the pure magnesium sample. The PCL peaks at 2θ equal to 21.3° and 23.6° are seen in all coated samples (PCL, PCL/2.5%HA, and PCL/5%HA). HA peaks are more distinctive in samples with the composite coating (PCL+HA) and especially in the sample with 5 wt.% of HA.

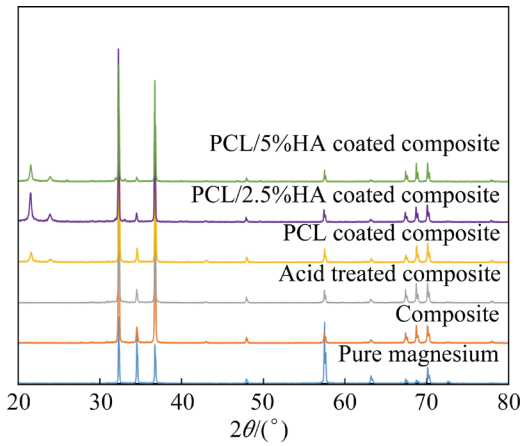

Fig. 5 XRD patterns for samples

Hydrophobicity reduces the possibility of corrosion in samples based on several studies. In contrast, this hydrophobic surface prevents bone cell adhesion, growth, and proliferation. PCL fibers are hydrophobic due to their low wettability. So, increasing the hydrophilicity of fibers by using HA particles with a hydrophilic nature leads to improved cell adhesion and growth [62−64]. Figure 6 illustrates the wettability of samples using distilled water droplets. Reduction of the contact angle occurred in the composite compared to the pure sample. This can be caused by the escalation in surface energy of the fine-grained composite surface [65] and the hydrophilic nature of the HA-reinforcing phase [40]. Further reduction of the angle in the acid-treated composite is apparent. The conversion coating forms a porous and hydrophilic $Mg(OH)_2$ phase on the surface. The hydrophilicity of this sample improves the adhesion quality of the fibers to the metal surface [66]. The PCL fiber-coated sample establishes the most hydrophobic surface (117°). A reduction in contact angle is observed with the addition of 2.5 wt.% HA into the PCL fibers due to the hydrophilic nature of HA. The PCL/5%HA coated composite has a smaller contact angle value.

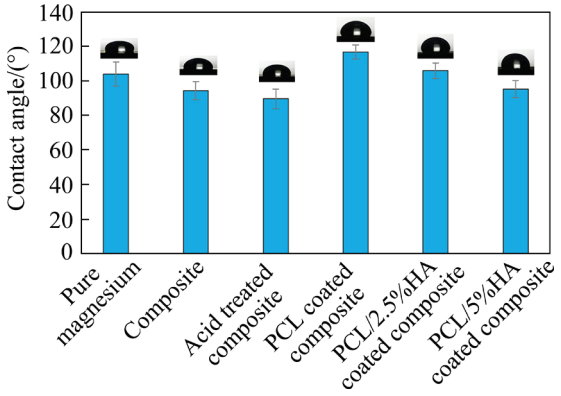

Fig. 6 Wettability of samples using distilled water droplets

3.2 Tensile and compressive properties

The addition of the reinforcing particles, depending on the size and material, enhances the strength of the sample in comparison to the base metal. The reinforcing mechanisms include the creation of high-density dislocation zones around particles due to differences in the matrix and reinforcements properties and the entrapment of dislocations by these particles. Also, the pinning effect of reinforcing particles during hot extrusion prevents the growth of nucleated grains. Load transfer and bearing by particles strengthen the material, too. The particle distribution should be homogeneous to improve the properties [65,67]. According to the particle distribution in Fig. 2, a boost in strength can be expected. However, the ductility is usually weaker than the pure material due to the rapid saturation of the hardening in composites [68,69]. Tensile and compressive stress−strain curves and mechanical properties for pure magnesium and 2.5% HA composite samples are presented in Fig. 7. The compressive yield strength for the composite is 151 MPa, which is in the range of compressive yield strength of cortical

bone (130−180) MPa [1]. It represents a 107% development over that of pure magnesium. The tensile yield strength of the composite is 172 MPa, which has augmented by 37% compared to that of pure magnesium. The ultimate strength values under compressive and tensile loads by 14% and 21% improvement over values of pure magnesium are 348 and 238 MPa, respectively. Likewise, the compressive and tensile fracture strains are 0.14 and 0.23, by a decrease of 8% and 26% compared to those of pure magnesium.

3.3 Corrosion behavior

3.3.1 Polarization test

Figure 8 shows the potentiodynamic polarization diagram for pure magnesium, composite, acid-treated composite, and samples coated with PCL, PCL/2.5%HA, and PCL/5%HA. The curves shifting to the left in these diagrams indicates a diminished corrosion current density and thus, improved corrosion resistance. The parameters extracted from the PDP diagram are given in Table 1. The composite sample exhibits a lower current density than the pure sample (354 μA/cm^2), due to fine-grain and proper distribution of HA, resulting in more uniform corrosion and accelerated passive layer formation [70]. A greater amount of HA raises agglomeration, cavities, and defects. Thus, fluid penetration and non-uniform corrosion occur [57,71]. Therefore, the enhancement in polarization resistance of composite approves the appropriate distribution of reinforcing particles. Acid treatment of the composite has lessened the current density to 257 μA/cm^2 due to creating a protective layer of $Mg(OH)_2$. It should be noted that the corrosion potential in composite and acid-coated samples is higher than that of pure magnesium (−1.51 and −1.45 V compared to −1.61 V). Increasing the corrosion potential indicates a drop-off in the tendency of the material to corrosion. These observations display the performance of the fabricated composite and the conversion coating with HNO_3. A much more significant decrease in corrosion current density is observed for the PCL, PCL/2.5%HA, and PCL/5%HA coated samples (9, 23, and 25 μA/cm^2, respectively). The coatings prevent rapid penetration and contact with the substrate for the SBF fluid and protect the surface. The most considerable current density reduction is seen in the PCL sample, which discloses a discount

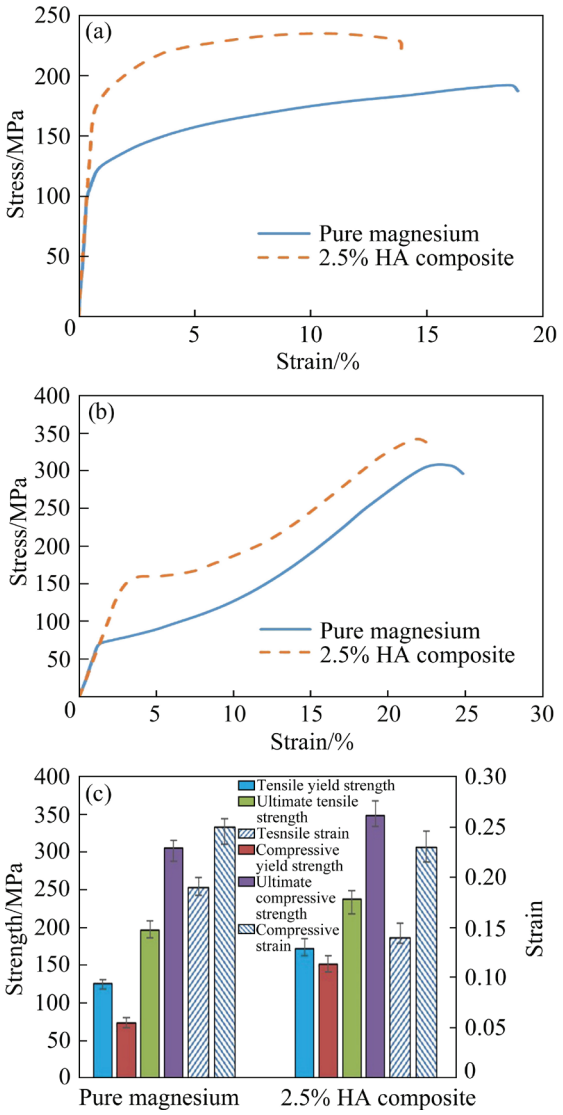

Fig. 7 Tensile (a) and compressive (b) stress−strain curves and mechanical properties (c) for pure magnesium and 2.5% HA composite samples

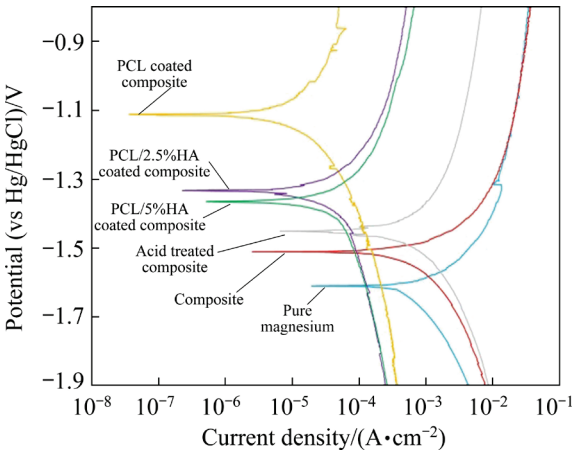

Fig. 8 Potentiodynamic polarization diagrams for pure magnesium, composite, acid-treated composite, and composites coated with PCL, PCL/2.5%HA, and PCL/5%HA

Table 1 Parameters extracted from PDP diagram

Sample	φ_{corr}/V	J_{corr}/(μA·cm^{-2})	β_a/(mV·dec^{-1})	β_c/(mV·dec^{-1})	R_p/(kΩ·cm^2)
Pure magnesium	−1.61	645	114	321	0.57
Composite	−1.51	354	92	173	0.74
Acid treated composite	−1.45	257	126	120	1.04
PCL coated composite	−1.12	9	169	118	33.52
PCL/2.5%HA coated composite	−1.34	23	170	207	17.62
PCL/5%HA coated composite	−1.36	25	158	203	15.43

of two orders of magnitude compared to the uncoated composite.

A potential gain is perspicuous for the sample with PCL coating. PCL/HA composite coatings change the pH of the environment by releasing HA during decomposition. So, they create different corrosion resistance compared to the sample with PCL coating by affecting the reaction and corrosion products. The larger current density in samples with PCL/HA composite coating can be due to the minor hydrophobicity of these samples, which causes more penetration of the body simulator fluid. Also, the PCL/5%HA sample presents a higher current density compared to the PCL/2.5%HA sample (25 μA/cm^2 vs 23 μA/cm^2). This may be caused by lower water contact angle and larger pores, according to Figs. 4 and 6. However, immersion studies are needed to evaluate the performance of these coatings better. Fiber coating increases corrosion resistance from less than 1 kΩ·cm^2 to more advanced values, even to 33.52 kΩ·cm^2.

3.3.2 Hydrogen evolution and pH variation

As magnesium degradation occurs, hydrogen gas is evolved according to $Mg + 2H_2O = Mg(OH)_2 + H_2$. The corrosion intensity can be estimated by calculating the exhaust gas. Corrosion of magnesium in SBF medium leads to other corrosion products along with MgO and $Mg(OH)_2$ due to various ions such as Cl^-, HPO_4^{2-}, HCO_3^-, and SO_4^{2-}. The $Mg(OH)_2$ layer is converted to high soluble $MgCl_2$ in the presence of Cl^- ions. Other mentioned ions can weaken the attacks of invading ions by forming deposits such as phosphate and carbonate layers. However, if the concentration is low, HCO_3^- will increase the corrosion rate of magnesium by consuming OH^- [72,73]. With the destruction of the protective layer, corrosion intensifies, and this process continues until the corrosion process slows down with increasing pH and deposition of stable products.

Figure 9(a) illustrates the cumulative H_2 evolution during the immersion of samples for 336 h (14 d) in the SBF medium. An intensive upsurge in the hydrogen release for uncoated samples can be seen during the early hours. Unprotected magnesium exposure allows for a rapid corrosion reaction, accelerating the release of hydrogen gas. Among these samples, the composite performed better than pure magnesium, especially in the acid-treated state. The final amount of H_2 reached 19.78 mL/cm^2 for the acid-treated composite, which was reduced by 21% compared to the pure sample. This is caused by the formation of

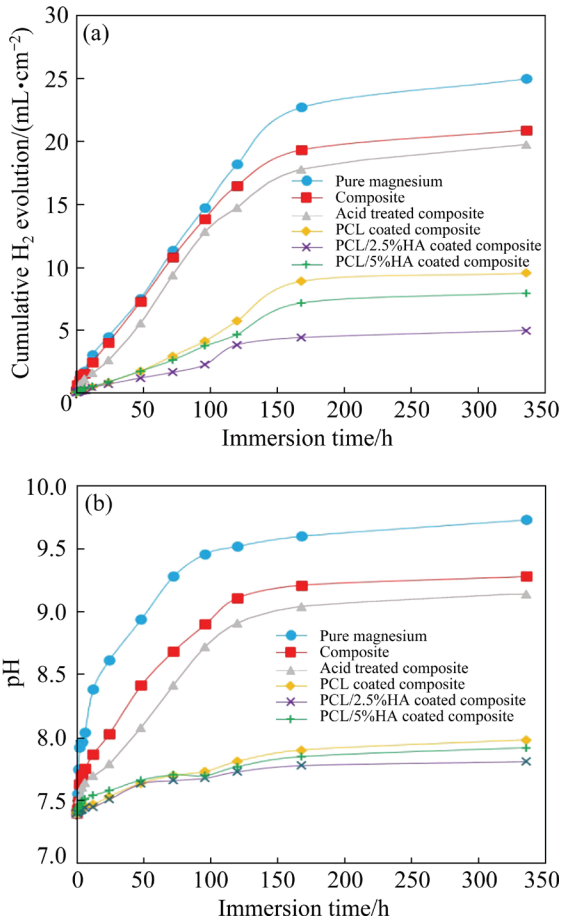

Fig. 9 Cumulative H_2 evolution (a), and pH variation (b) during immersion of samples for 336 h (14 d)

a protective layer of $Mg(OH)_2$ and thus better performance against the attack of destructive ions such as Cl^-. In the case of coated specimens, the rate of H_2 evolution is much lower than that of uncoated specimens. Penetration of the fluid is prevented due to the hydrophobicity of coating. The amount of hydrogen released for coated samples is approximately the same for about 24 h. But over time, it proves the effect of the presence of HA among the PCL fibers. These particles further improve corrosion resistance by increasing bio-mineralization and modifying precipitated products (deposition of more Ca−P compounds). The PCL/2.5%HA coated sample has an H_2 evolution of 5 mL/cm^2 after 14 d, which is lessened by 48% compared to the PCL coated sample. In the PCL/5%HA sample, more fluid penetration causes more corrosion as a consequence of increased pore diameter and also less hydrophobicity. The final amount of evolved H_2 in this sample is 7.95 mL/cm^2, which is 17% less than the sample with PCL coating.

Figure 9(b) depicts the pH variation during the immersion of the samples. With released hydrogen, magnesium corrosion causes a rise in pH by releasing OH^- ions. This pH increment was tremendous for uncoated pure magnesium and two composite samples. Pure magnesium experienced severe corrosion from the beginning, resulting in a sharp rise in pH. After 96 h, the pH value reached about 9.5 and then augmented to the final value of 9.8. The composite sample resisted much better against corrosion due to the advantages of HA in its structure. The acidification of this composite by creating a protective layer, especially in the early times, has caused the pH value to reach about 9. It is less than that of the pure magnesium sample after 120 h, and the pH value remained almost constant until the 14th day. The pH value raised to about 7.98 after 14 d for the PCL-coated sample. In the PCL/2.5%HA sample, which performed better, the pH increment was limited to 7.8 after 14 d. This indicates that the PCL fiber coating and its composition are able to protect the metal surface well against the penetration of SBF. The pH value in the PCL/5%HA sample also reached 7.92, slightly higher than that of PCL/2.5%HA coated sample.

Figure 10 illustrates the SEM image of the samples after exposure to SBF for 1, 3, 7, and 14 d. As predicted from the pH and hydrogen release diagrams, the pure magnesium sample demonstrates severe corrosion from Day 1. The attack of destructive ions causes pitting, and with the penetration of SBF, extensive corrosion causes surface cracking. In composite and acid-treated composite, the damage is much more minor until Day 3, and superficial cracks can be seen on the surface. More surface degradation occurs due to the peeling of the upper $Mg(OH)_2$ converted layer with increasing exposure time, resulting in fluid infiltration. SBF penetration happens with a delay in the acid-treated sample, although SEM images indicate that uncoated samples exposed to SBF have a high corrosion rate and need to be coated.

According to Fig. 10, the adhesion of the coating is maintained in all coated samples until the 14th day. The corrosion products appear on these coatings after exposure intervals. The main part of these products can be seen in Day 7 and Day 14, indicating that the corrosion was not severe until the third day due to the protection of the $Mg(OH)_2$ layer. The amount of the products in the PCL coated sample is more than that of the other two coatings. The presence of HA and stimulation of Ca−P absorption could be the reason. Corrosion products on samples after the 7th day represent that the corrosion becomes uniform after this exposure period. On Day 14, the surface of PCL/2.5%HA coated sample displays small corrosion products. This indicates the effectiveness of this type of coating. Although the PCL/5%HA sample exhibits less corrosion than the sample with PCL coating, more and larger corrosion products are seen on its surface. The schematic illustration of the apatite formation of PCL/HA nanofiber-coated Mg alloy after immersion in SBF is presented in Fig. 11.

Figure 12 represents the SEM image of the samples from a closer view after 14 d of immersion in the SBF medium, along with the EDS diagram of products. Pure magnesium sample cannot absorb Ca−P products and exhibits only a weak peak of Ca. The Cl peak is clearly seen in this sample, which indicates the attack of Cl^- and the destruction of the $Mg(OH)_2$ layer. Cl peak is smaller in the composite sample and almost not seen on the acid-treated composite sample. The peaks of Ca and P are observed on composite and acid-treated composite, which indicates bio-mineralization in these samples. The adsorption of Ca−P products is also determined

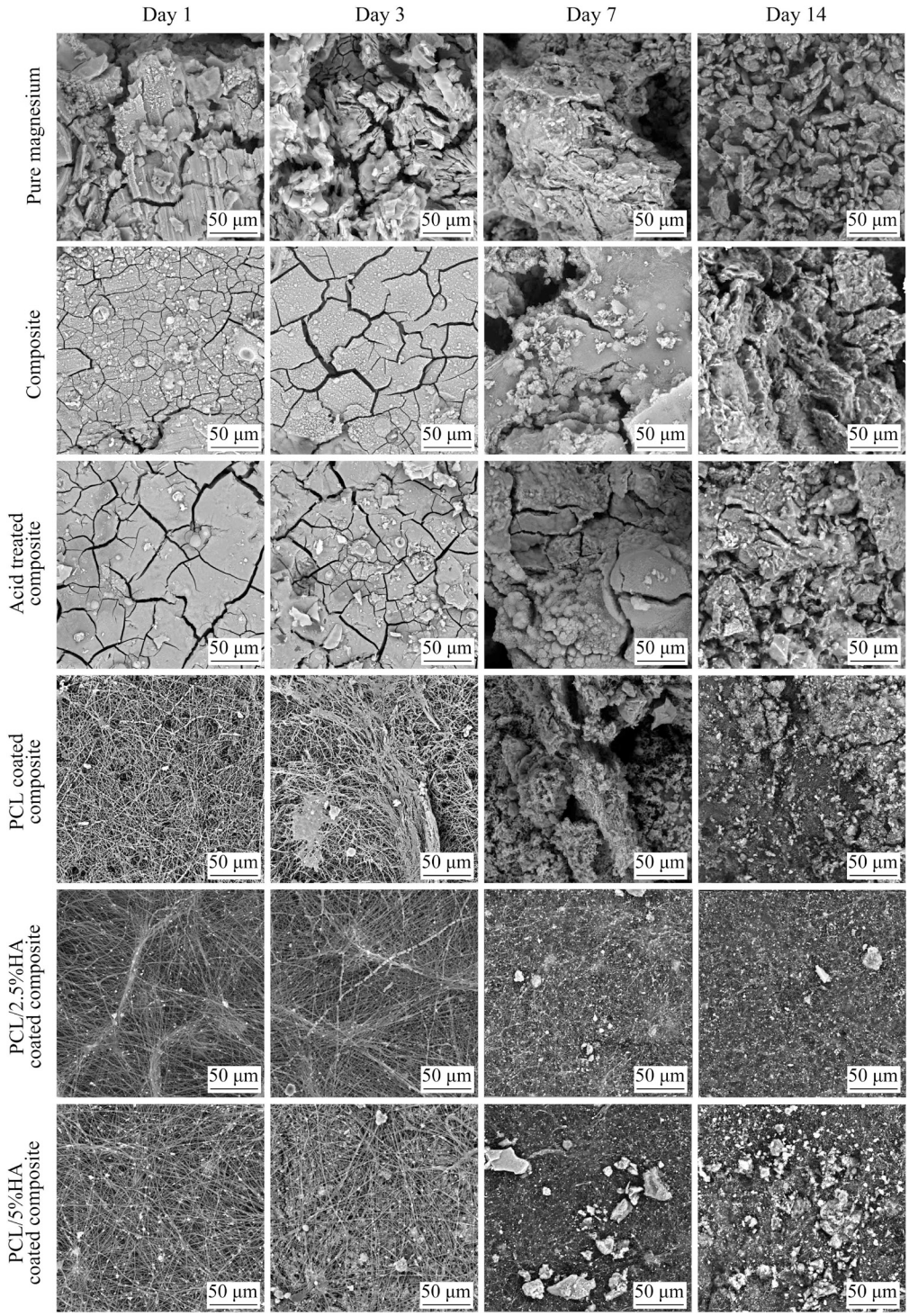

Fig. 10 SEM images of samples after exposure to SBF for 1, 3, 7, and 14 d

by the peaks of these two elements in coated samples. The PCL-coated specimen demonstrates surpassing peaks and Cl percentages compared to composite-coating specimens. Due to the absence of HA in the structure of the fibers, it has shown less bio-mineralization capability. Also, the mass fraction of Ca and P in surface products of PCL/5%HA and PCL/2.5%HA samples is higher than that in the sample with PCL coating. Meanwhile, the molar ratio of Ca/P in the PCL/2.5%HA coated sample is about 1.67. This suggests that the coating is reasonable, and its Ca−P products are close to HA composition.

3.3.3 In vitro decomposition rate

Figure 13 depicts the corrosion rate diagram for the samples after immersion in the SBF for intervals of 6, 12, 24, 72, 168, and 336 h. The pure magnesium sample has the highest corrosion rate.

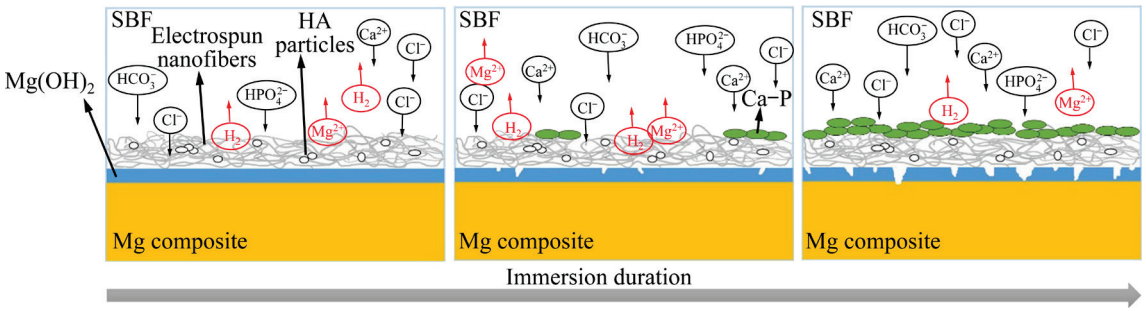

Fig. 11 Schematic illustration of apatite formation of PCL/HA nanofiber-coated Mg composite after immersion in SBF

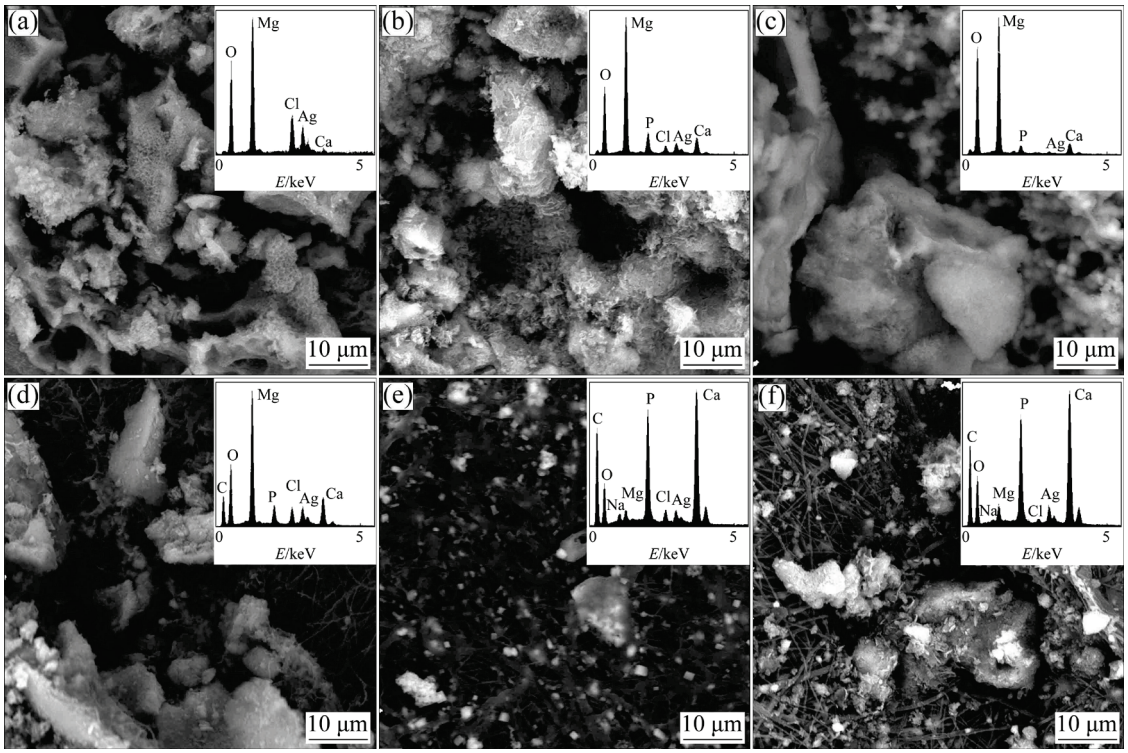

Fig. 12 SEM images of pure magnesium (a), composite (b), acid treated composite (c), PCL-coated (d), PCL/2.5%HA coated (e), and PCL/5%HA coated (f) composites after exposure to SBF for 14 d

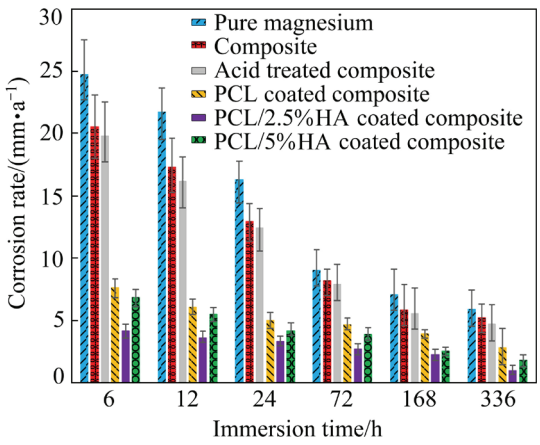

Fig. 13 Corrosion rates for samples after immersion in SBF for intervals of 6, 12, 24, 72, 168, and 336 h

The corrosion rate of this sample is greater than 5 mm/a after 336 h of exposure to the SBF. When placed in SBF, only a thin layer of $Mg(OH)_2$ is formed, which is quickly peeled off. Composite and acid-treated samples have lower corrosion rates. The acid-treated composite sample demonstrates a corrosion rate of 4.77 mm/a after 336 h of immersion. HA in the structure and surface of the material and acid treatment of the composite increases the corrosion resistance by forming a suitable protective layer. However, the effect of this layer has diminished over a more extended period with destruction by invasive ions. PCL and PCL/HA-coated samples reveal good resistance from the beginning. Corrosion rates below 5 mm/a

result from PCL/2.5%HA sample at all intervals. Support of the protective layer created by the acid, the capillary action, and the deposition of beneficial Ca−P compounds on the surface leads to superior resistance. Composite coatings perform better than PCL coatings for longer exposure intervals in the SBF. The function of HA particles among fibers structure in absorbing Ca−P products and strengthening the protective layer is evident. PCL/2.5%HA sample has the lowest corrosion rate with an average value of 0.98 mm/a after 336 h. It represents an 81% dwindle compared to the uncoated composite.

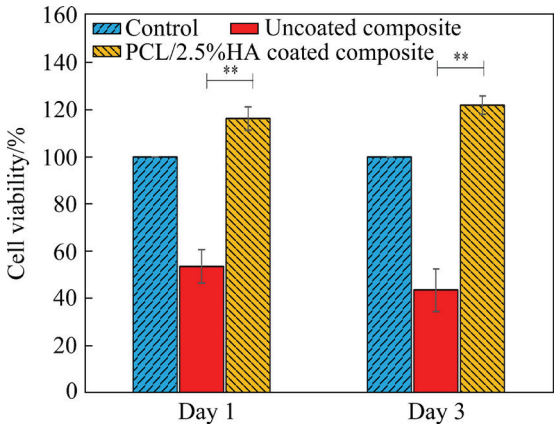

Fig. 14 MTT assay results for uncoated composite and PCL/2.5%HA coated composite using MC3T3-E1 cells (**$p < 0.01$)

3.4 Cell biocompatibility

The results of the MTT test on MC3T3-E1 cells for uncoated and PCL/2.5%HA coated composites are shown in Fig. 14. The lowest biocompatibility was determined for the uncoated composite, which is 53% and 42% in 1 and 3 d periods, respectively. PCL/2.5%HA fiber coating significantly enhances cell viability in 1 d as well as 3 d periods. In this regard, significant differences were observed between the viability values of the composite and the PCL/2.5%HA coated composite samples (p<0.01). As can be seen from Fig. 15, the uncoated composite was not able to create cell adhesion. However, the PCL/2.5%HA coated sample presents good adhesion due to its porous structure, specific surface, and presence of HA. Other studies have also demonstrated the favorable

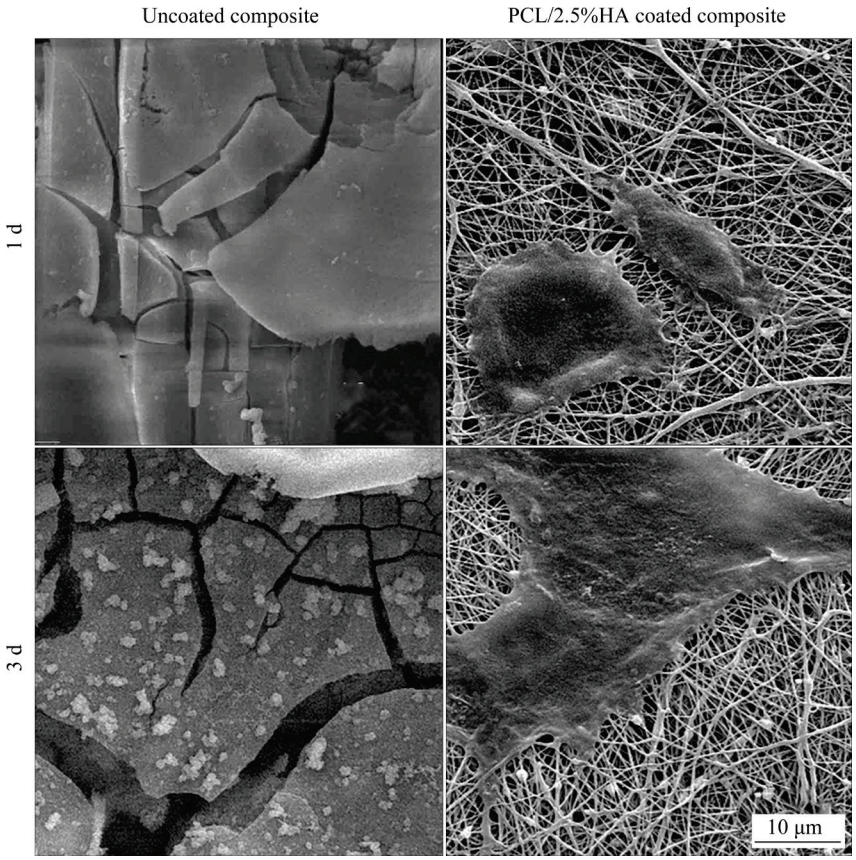

Fig. 15 SEM images after cell culture on uncoated composite and PCL/2.5%HA coated composite for 1 and 3 d

effect of HA on biocompatibility [40,41]. The spread of cells on the third day is evident on the surface of the fibers. Composite surface instability, pH rise, and hydrogen evolution due to corrosion result in this sample having lower biocompatibility than the coated sample.

4 Conclusions

(1) Proper distribution of HA in the fabricated composite escalates the compressive yield strength of the composite by 107% compared to that of pure magnesium.

(2) The addition of HA and acid treatment diminish the corrosion current density by 60% compared to that of pure magnesium.

(3) All coated specimens show higher corrosion resistance compared to the uncoated ones. PCL coating reduces the corrosion current density of the sample by two orders of magnitude.

(4) The PCL/2.5%HA sample has the lowest corrosion rate of 0.98 mm/a in 14 d, by a reduction of 81% compared to the uncoated composite.

(5) The PCL/2.5%HA fiber coating increases significantly cell viability in 1 d as well as 3 d periods. It also exhibits proper adhesion due to its porous structure, specific surface, and presence of HA.

CRediT authorship contribution statement

M. SHAMSI: Conceptualization, Methodology, Investigation, Writing − Original draft preparation; **M. SEDIGHI:** Supervision, Project administration, Writing − Review & editing; **A. BAGHERI:** Resources, Investigation, Visualization.

Declaration of competing interest

The authors declare that they have no known competing financial interests or personal relationships that could have appeared to influence the work reported in this paper.

References

[1] UPPAL G, THAKUR A, CHAUHAN A, BALA S. Magnesium based implants for functional bone tissue regeneration—A review [J]. Journal of Magnesium and Alloys, 2022, 10: 356−386.

[2] SHIRI M, JAFARI H, SINGH R. Effect of extrusion parameters on degradation of magnesium alloys for bioimplant applications: A review [J]. Transactions of Nonferrous Metals Society of China, 2022, 32: 2787–2813.

[3] LI C M, GUO C C, FITZPATRICK V, IBRAHIM A, ZWIERSTRA M J, HANNA P, LECHTIG A, NAZARIAN A, LIN S J, KAPLAN D L. Design of biodegradable, implantable devices towards clinical translation [J]. Nature Reviews Materials, 2020, 5: 61−81.

[4] BAKHSHESHI-RAD H R, DAYAGHI E, ISMAIL A F, MADZLAN A, AKHAVAN-FARID A, XIONGBIAO C. Synthesis and in-vitro characterization of biodegradable porous magnesium-based scaffolds containing silver for bone tissue engineering [J]. Transactions of Nonferrous Metals Society of China, 2019, 29: 984−996.

[5] BROOKS E K, EHRENSBERGER M T. Bio-corrosion of magnesium alloys for orthopaedic applications [J]. Journal of Functional Biomaterials, 2017, 8: 38.

[6] WAN P, TAN L L, YANG K. Surface modification on biodegradable magnesium alloys as orthopedic implant materials to improve the bio-adaptability: A review [J]. Journal of Materials Science & Technology, 2016, 32: 827−834.

[7] ZHAO C Y, PAN F S, PAN H C. Microstructure, mechanical and bio-corrosion properties of as-extruded Mg−Sn−Ca alloys [J]. Transactions of Nonferrous Metals Society of China, 2016, 26: 1574−1582.

[8] WANG X J, ZHANG Y B, GUO E Y, CHEN Z N, KANG H J, LIU X Q, HAN P, WANG T M. In vitro investigation on microstructure, bio-corrosion properties and cytotoxicity of as-extruded Mg−5Sn−*x*In alloys [J]. Journal of Alloys and Compounds, 2021, 877: 160294.

[9] XIA Y, WU L, YAO W H, HAO M, CHEN J, ZHANG C, WU T, XIE Z H, SONG J F, JIANG B, MA Y L, PAN F S. In-situ layered double hydroxides on Mg−Ca alloy: Role of calcium in magnesium alloy [J]. Transactions of Nonferrous Metals Society of China, 2021, 31: 1612−1627.

[10] KASAEIAN-NAEINI M, SEDIGHI M, HASHEMI R. Severe plastic deformation (SPD) of biodegradable magnesium alloys and composites: A review of developments and prospects [J]. Journal of Magnesium and Alloys, 2022, 10: 938−955.

[11] LIU B S, CAO M M, ZHANG Y Z, HU Y, GONG C W, HOU L F, WEI Y H. Microstructure, anticorrosion, biocompatibility and antibacterial activities of extruded Mg−Zn−Mn strengthened with Ca [J]. Transactions of Nonferrous Metals Society of China, 2021, 31: 358−370.

[12] MAKKAR P, KANG H J, PADALHIN A R, FARUQ O, LEE B. In-vitro and in-vivo evaluation of strontium doped calcium phosphate coatings on biodegradable magnesium alloy for bone applications [J]. Applied Surface Science, 2020, 510: 145333.

[13] YU K, LI P, HAN Q, WANG Q, KARPUSHENKOV S A, LU X P, IGNATENKO O V. Investigation of biodegradability, cytocompatibility and antibacterial property of plasma electrolytic oxidation coating on Mg [J]. Surfaces and Interfaces, 2022, 30: 101840.

[14] PANDEY A, MIDHA S, SHARMA R K, MAURYA R, NIGAM V K, GHOSH S, BALANI K. Antioxidant and antibacterial hydroxyapatite-based biocomposite for orthopedic applications [J]. Materials Science and Engineering C, 2018, 88: 13−24.

[15] ZHOU Z W, ZHENG B, GU Y P, SHEN C, WEN J, MENG Z B, CHEN S P, OU J, QIN A M. New approach for improving anticorrosion and biocompatibility of magnesium alloys via polydopamine intermediate layer-induced hydroxyapatite coating [J]. Surfaces and Interfaces, 2020, 19: 100501.

[16] KUMAR K, DAS A, PRASAD S B. Recent developments in biodegradable magnesium matrix composites for orthopaedic applications: A review based on biodegradability, mechanical and biocompatibility perspective [J]. Materials Today: Proceedings, 2021, 44: 2038−2042.

[17] SUNIL B R, KUMAR T S S, CHAKKINGAL U, NANDAKUMAR V, DOBLE M. Friction stir processing of magnesium−nanohydroxyapatite composites with controlled in vitro degradation behavior [J]. Materials Science and Engineering C, 2014, 39: 315−324.

[18] JAISWAL S, DUBEY A, LAHIRI D. In vitro biodegradation and biocompatibility of Mg−HA-based composites for orthopaedic applications: A review [J]. Journal of the Indian Institute of Science, 2019, 99: 303−327.

[19] WAN P, YAN X D, LI M, ZHAO M C, ZHANG Y, YANG K. Construction of bio-functional Mg/HA composite layered coating for orthopedic application [J]. Science China Technological Sciences, 2021, 64: 2541−2550.

[20] DEHGHANGHADIKOLAEI A, FOTOVVATI B. Coating techniques for functional enhancement of metal implants for bone replacement: A review [J]. Materials, 2019, 12: 1795.

[21] YIN Z Z, QI W C, ZENG R C, CHEN X B, GU C D, GUAN S K, ZHENG Y F. Advances in coatings on biodegradable magnesium alloys [J]. Journal of Magnesium and Alloys, 2020, 8: 42−65.

[22] WU G, IBRAHIM J M, CHU P K. Surface design of biodegradable magnesium alloys—A review [J]. Surface and Coatings Technology, 2013, 233: 2−12.

[23] LI L Y, CUI L Y, ZENG R C, LI S Q, CHEN X B, ZHENG Y, KANNAN M B. Advances in functionalized polymer coatings on biodegradable magnesium alloys—A review [J]. Acta Biomaterialia, 2018, 79: 23−36.

[24] ROUEIN Z, JAFARI H, PISHBIN F, MOHAMMADI R, SIMCHI A. Biodegradation behavior of polymethyl methacrylate−bioactive glass 45S5 composite coated magnesium in simulated body fluid [J]. Transactions of Nonferrous Metals Society of China, 2022, 32: 2216−2228.

[25] ZHANG A M, LENIN P, ZENG R C, KANNAN M B. Advances in hydroxyapatite coatings on biodegradable magnesium and its alloys [J]. Journal of Magnesium and Alloys, 2022, 10: 1154−1170.

[26] ZHAO D P, SHI W, SHANG P, NIE H M, ZHANG Y, TANG J C. Effects of Sr incorporation on surface structure and corrosion resistance of hydroxyapatite coated Mg−4Zn alloy for biomedical applications [J]. Transactions of Nonferrous Metals Society of China, 2018, 28: 1563−1570.

[27] BAKHSHESHI-RAD H R, HAMZAH E, ISMAIL A F, AZIZ M, KARAMIAN E, IQBAL N. Bioactivity, in-vitro corrosion behavior, and antibacterial activity of silver−zeolites doped hydroxyapatite coating on magnesium alloy [J]. Transactions of Nonferrous Metals Society of China, 2018, 28: 1553−1562.

[28] OMER S, FORGÁCH L, ZELKÓ R, SEBE I. Scale-up of electrospinning: Market overview of products and devices for pharmaceutical and biomedical purposes [J]. Pharmaceutics, 2021, 13: 286.

[29] XUE J J, WU T, DAI Y Q, XIA Y N. Electrospinning and electrospun nanofibers: Methods, materials, and applications [J]. Chemical Reviews, 2019, 119: 5298−5415.

[30] VURAT M T, ELÇIN A E, ELÇIN Y M. Osteogenic composite nanocoating based on nanohydroxyapatite, strontium ranelate and polycaprolactone for titanium implants [J]. Transactions of Nonferrous Metals Society of China, 2018, 28: 1763−1773.

[31] BAKHSHESHI-RAD H R, ISMAIL A F, AZIZ M, AKBARI M, HADISI Z, KHOSHNAVA S M, PAGAN E, CHEN X. Co-incorporation of graphene oxide/silver nanoparticle into poly-L-lactic acid fibrous: A route toward the development of cytocompatible and antibacterial coating layer on magnesium implants [J]. Materials Science and Engineering C, 2020, 111: 110812.

[32] BAKHSHESHI-RAD H R, AKBARI M, ISMAIL A F, AZIZ M, HADISI Z, PAGAN E, DAROONPARVAR M, CHEN X. Coating biodegradable magnesium alloys with electrospun poly-L-lactic acid-åkermanite-doxycycline nanofibers for enhanced biocompatibility, antibacterial activity, and corrosion resistance [J]. Surface and Coatings Technology, 2019, 377: 124898.

[33] ABDAL-HAY A, BARAKAT N A M, LIM J K. Influence of electrospinning and dip-coating techniques on the degradation and cytocompatibility of Mg-based alloy [J]. Colloids and Surfaces A: Physicochemical and Engineering Aspects, 2013, 420: 37−45.

[34] ZHANG W T, CHEN Y Q, CHEN M Y, ZHAO S, MAO J L, QU A, LI W, ZHAO Y C, HUANG N, WAN G J. Strengthened corrosion control of poly (lactic acid) (PLA) and poly (ε-caprolactone) (PCL) polymer-coated magnesium by imbedded hydrophobic stearic acid (SA) thin layer [J]. Corrosion Science, 2016, 112: 327−337.

[35] DASH T K, KONKIMALLA V B. Polymeric modification and its implication in drug delivery: poly-ε-caprolactone (PCL) as a model polymer [J]. Molecular Pharmaceutics, 2012, 9: 2365−2379.

[36] WANG Y, LIU Y Z, QIAN Y F, LV L H, LI X Y, LIU Y J. Characteristics of MgO/PCL/PVP antibacterial nanofiber membranes produced by electrospinning technology [J]. Surfaces and Interfaces, 2022, 28: 101661.

[37] YADI M, ESFAHANI H, NOURIAN A, NAVARD S H, FATTAH-ALHOSSEINI A. Surface modification of CP-Ti by calcium-phosphate via an integrated electrospinning and rapid heating and cooling (EMRHC) process: Essential in-vitro studies for bone regeneration [J]. Surfaces and Interfaces, 2021, 27: 101480.

[38] HANAS T, SAMPATH KUMAR T S, PERUMAL G, DOBLE M. Tailoring degradation of AZ31 alloy by surface pre-treatment and electrospun PCL fibrous coating [J]. Materials Science and Engineering C, 2016, 65: 43−50.

[39] KIM J, MOUSA H M, PARK C H, KIM C S. Enhanced corrosion resistance and biocompatibility of AZ31 Mg alloy using PCL/ZnO NPs via electrospinning [J]. Applied Surface Science, 2017, 396: 249−258.

[40] HANAS T, KUMAR T S S, PERUMAL G, DOBLE M, RAMAKRISHNA S. Electrospun PCL/HA coated friction stir processed AZ31/HA composites for degradable implant applications [J]. Journal of Materials Processing Technology, 2018, 252: 398−406.

[41] REZK A I, MOUSA H M, LEE J, PARK C H, KIM C S. Composite PCL/HA/simvastatin electrospun nanofiber coating on biodegradable Mg alloy for orthopedic implant application [J]. Journal of Coatings Technology and Research, 2019, 16: 477−489.

[42] BAKHSHESHI-RAD H R, ISMAIL A F, AZIZ M, HADISI Z, OMIDI M, CHEN X. Antibacterial activity and corrosion resistance of Ta_2O_5 thin film and electrospun PCL/MgO−Ag nanofiber coatings on biodegradable Mg alloy implants [J]. Ceramics International, 2019, 45: 11883−11892.

[43] PANAHI Z, TAMJID E, REZAEI M. Surface modification of biodegradable AZ91 magnesium alloy by electrospun polymer nanocomposite: Evaluation of in vitro degradation and cytocompatibility [J]. Surface and Coatings Technology, 2020, 386: 125461.

[44] NANDHINI G, NIVEDHA B, PRANESH M, KARTHEGA M. Study of polycaprolactone/curcumin loaded electrospun nanofibers on AZ91 magnesium alloy [J]. Materials Today: Proceedings, 2020, 33: 2170−2173.

[45] KARTHEGA M, PRANESH M, POONGOTHAI C, SRINIVASAN N. Poly caprolactone/titanium dioxide nanofiber coating on AM50 alloy for biomedical application [J]. Journal of Magnesium and Alloys, 2021, 9: 532−547.

[46] SABET A S, JABBARI A H, SEDIGHI M. Microstructural properties and mechanical behavior of magnesium/ hydroxyapatite biocomposite under static and high cycle fatigue loading [J]. Journal of Composite Materials, 2018, 52: 1711−1722.

[47] KOKUBO T, TAKADAMA H. How useful is SBF in predicting in vivo bone bioactivity? [J]. Biomaterials, 2006, 27: 2907−2915.

[48] ASTM G 59—97: Standard test method for conducting potentiodynamic polarization resistance measurements [S]. 2009.

[49] GAUR S, RAMAN R K S, KHANNA A S. In vitro investigation of biodegradable polymeric coating for corrosion resistance of Mg−6Zn−Ca alloy in simulated body fluid [J]. Materials Science and Engineering C, 2014, 42: 91−101.

[50] ASTM G 31 — 72: Standard practice for laboratory immersion corrosion testing of metals [S]. 2004.

[51] CHENG Y, HUANG L H, WANG Y C, HUO Q Y, SHAO Y H, BAO H J, LI Z Y, LIU Y D, LI X. Strontium promotes osteogenic differentiation by activating autophagy via the the AMPK/mTOR signaling pathway in MC3T3-E1 cells [J]. International Journal of Molecular Medicine, 2019, 44: 652−660.

[52] CHEN Y N, SUN C H, LU J, ZOU L, HU M W, YANG Z Y, XU Y Z. MicroRNA-590-5p antagonizes the inhibitory effect of high glucose on osteoblast differentiation by suppressing Smad7 in MC3T3-E1 cells [J]. Journal of International Medical Research, 2019, 47: 1740−1748.

[53] MIAO J L, JUE LIU, WANG H F, YANG H L, RUAN J M. Preparation of porous Ta−10%Nb alloy scaffold and its in vitro biocompatibility evaluation using MC3T3-E1 cells [J]. Transactions of Nonferrous Metals Society of China, 2018, 28: 2053−2061.

[54] BOMMALA V K, KRISHNA M G, RAO C T. Magnesium matrix composites for biomedical applications: A review [J]. Journal of Magnesium and Alloys, 2019, 7: 72−79.

[55] KHORASHADIZADE F, ABAZARI S, RAJABI M, BAKHSHESHI-RAD H R, ISMAIL A F, SHARIF S, RAMAKRISHNA S, BERTO F. Overview of magnesium−ceramic composites: Mechanical, corrosion and biological properties [J]. Journal of Materials Research and Technology, 2021, 15: 6034−6066.

[56] WITTE F, FEYERABEND F, MAIER P, FISCHER J, STÖRMER M, BLAWERT C, DIETZEL W, HORT N. Biodegradable magnesium−hydroxyapatite metal matrix composites [J]. Biomaterials, 2007, 28: 2163−2174.

[57] KHALAJABADI S Z, KADIR M R A, IZMAN S, MARVIBAIGI M. The effect of MgO on the biodegradation, physical properties and biocompatibility of a Mg/HA/MgO nanocomposite manufactured by powder metallurgy method [J]. Journal of Alloys and Compounds, 2016, 655: 266−280.

[58] AMIRKHANLOU S, NIROUMAND B. Synthesis and characterization of 356-SiC_p composites by stir casting and compocasting methods [J]. Transactions of Nonferrous Metals Society of China, 2010, 20(Suppl.): s788−s793.

[59] AHMED M K, RAMADAN R, EL-DEK S I, USKOKOVIĆ V. Complex relationship between alumina and selenium-doped carbonated hydroxyapatite as the ceramic additives to electrospun polycaprolactone scaffolds for tissue engineering applications [J]. Journal of Alloys and Compounds, 2019, 801: 70−81.

[60] BANIMOHAMAD-SHOTORBANI B, RAHMANI D E L, BAKHSHAYESH A, MEHDIPOUR A, JAROLMASJED S, SHAFAEI H. The efficiency of PCL/HAp electrospun nanofibers in bone regeneration: A review [J]. Journal of Medical Engineering & Technology, 2021, 45: 511−531.

[61] LIAO G Y, JIANG S B, XU X J, KE Y L. Electrospun aligned PLLA/PCL/HA composite fibrous membranes and their in vitro degradation behaviors [J]. Materials Letters, 2012; 82: 159−162.

[62] KUANG J, BA Z X, LI Z Z, WANG Z Z, QIU J H. The study on corrosion resistance of superhydrophobic coatings on magnesium [J]. Applied Surface Science, 2020, 501: 144137.

[63] JO S, KANG S M, PARK S A, KIM W D, KWAK J, LEE H. Enhanced adhesion of preosteoblasts inside 3D PCL scaffolds by polydopamine coating and mineralization [J]. Macromolecular Bioscience, 2013, 13: 1389−1395.

[64] HASSAN M I, SULTANA N, HAMDAN S. Bioactivity assessment of poly (ε-caprolactone)/hydroxyapatite electrospun fibers for bone tissue engineering application [J]. Journal of Nanomaterials, 2014, 2014: 573238.

[65] SHEN M J, WANG X J, YING T, WU K, SONG W J. Characteristics and mechanical properties of magnesium matrix composites reinforced with micron/submicron/nano SiC particles [J]. Journal of Alloys and Compounds, 2016, 686: 831−840.

[66] RAHIM S A, RABEEH V P M, JOSEPH M A, HANAS T. Does acid pickling of Mg−Ca alloy enhance

biomineralization? [J]. Journal of Magnesium and Alloys, 2021, 9: 1028−1038.
[67] YANG H, TOPPING T D, WEHAGE K, JIANG L, LAVERNIA E J, SCHOENUNG J M. Tensile behavior and strengthening mechanisms in a submicron B_4C-reinforced Al trimodal composite [J]. Materials Science and Engineering A, 2014, 616: 35−43.
[68] LIU J L, HUANG X Y, ZHAO K, ZHU Z W, ZHU X X, AN L N. Effect of reinforcement particle size on quasistatic and dynamic mechanical properties of Al−Al_2O_3 composites [J]. Journal of Alloys and Compounds, 2019, 797: 1367−1371.
[69] ADEOSUN S O, AKPAN E I, GBENEBOR O P, BALOGUN S A. Ductility and hardness of chloride cleaned AA6011/SiC_p composites [J]. Transactions of Nonferrous Metals Society of China, 2016, 26: 339−347.
[70] LIU D B, XU G Q, JAMALI S S, ZHAO Y, CHEN M F, JURAK T. Fabrication of biodegradable HA/Mg−Zn−Ca composites and the impact of heterogeneous microstructure on mechanical properties, in vitro degradation and cytocompatibility [J]. Bioelectrochemistry, 2019, 129: 106−115.
[71] GUO Y T, LI G Y, XU Y C, XU Z Z, GANG M Q, SUN G X, ZHANG Z H, YANG X H, YU Z L, LIAN J S, REN L Q. The microstructure, mechanical properties, corrosion performance and biocompatibility of hydroxyapatite reinforced ZK61 magnesium-matrix biological composite [J]. Journal of the Mechanical Behavior of Biomedical Materials, 2021, 123: 104759.
[72] XIN Y, HU T, CHU P K. In vitro studies of biomedical magnesium alloys in a simulated physiological environment: A review [J]. Acta Biomaterialia, 2011, 7: 1452−1459.
[73] ZALUDIN M A F, JAMAL Z A Z, DERMAN M N, KASMUIN M Z. Corrosion analysis of hydroxyapatite coated magnesium in simulated body fluid (SBF), phosphate buffered saline (PBS), and Ringer's solution [J]. Materials Today: Proceedings, 2019, 16: 1686−1691.

PCL/HA 静电纺丝纤维涂层对可降解 Mg/HA 复合材料的表面改性：力学性能、腐蚀和生物相容性

M. SHAMSI, M. SEDIGHI, A. BAGHERI

School of Mechanical Engineering, Iran University of Science and Technology, Tehran, Iran

摘　要：采用搅拌铸造和挤压法制备 Mg/HA 复合材料，并在其表面采用静电纺丝法涂覆聚己内酯/羟基磷灰石(PCL/HA)纤维(2.5%和 5% HA，质量分数)，以提高其耐腐蚀性。力学性能测试结果表明，复合材料的压缩屈服强度从 73 MPa(纯镁)提高到 151 MPa，提高了 107%。SEM、EDS 和 XRD 分析表明，HA 颗粒分布在多孔涂层中。极化曲线结果表明，涂层试样的耐腐蚀性能均优于未涂覆试样。PCL 涂层使样品的腐蚀电流密度降低了两个数量级。通过极化和体外腐蚀试验证明了 HA 在涂层中的有效性。涂层和随后形成的 Ca−P 层阻碍了模拟体液与基体的接触和渗透，从而起到保护表面的作用。PCL/2.5%HA 涂层样品的腐蚀速率最低，其平均值为 0.98 mm/a，与未涂层样品相比，在 14 天内减少了 81% 。根据 3 天 MTT 结果，使用 PCL/2.5%HA 涂层可使细胞活性从 43%提高到 121%。综上，涂覆 PCL/2.5%HA 纤维的 Mg/HA 复合材料在生物可吸收植入物方面具有广阔的应用前景。

关键词：镁基复合材料；复合涂层；生物可降解；羟基磷灰石；聚己内酯纤维

(Edited by Bing YANG)